In-lab ALOHA mid-infrared up-conversion interferometer in the photon counting regime @$\lambda = 3.39$ μm

Ludovic Szemendera, Ludovic Grossard, Laurent Delage, François Reynaud

MNRAS **000**, 1–6 (2017) Preprint March 24, 2017 Compiled using MNRAS LATEX style file v3.0

In-lab ALOHA mid-infrared up-conversion interferometer in the photon counting regime @λ = 3.39 µm

L. Szemendera, L. Grossard, L. Delage and F. Reynaud★
Xlim, Département Photonique, Université de Limoges, UMR CNRS 7252, 123 Av. Albert Thomas, 87060 Limoges CEDEX, France

Accepted XXX. Received YYY; in original form ZZZ

ABSTRACT
Astronomical Light Optical Hybrid Analysis (ALOHA@3.39 µm) is a new instrumental concept designed for high angular resolution astronomical imaging in the *L* Band. The originality of our experimental device is to include a frequency conversion process in each arm of the interferometer that frequency shifts the mid infrared signal to the near infrared domain. This method relaxes the stringent limitations due to the thermal noise background radiated by the instrument itself. The aim of this paper is to estimate the current sensitivity limit of the instrument and validate the ability to provide calibrated contrasts with a quasi monochromatic signal. We demonstrate the possibility to measure fringe contrasts greater than 94.5% with a signal-to-noise ratio close to 7. The flux level at the input of each arm of the interferometer is then equal to 100 fW. This would correspond to a zero magnitude star in the *L* Band for a 1 m^2 telescope surface and a 3 nm converted spectral bandwidth.

Key words: Instrumentation: high angular resolution – techniques: interferometric.

1 INTRODUCTION

Astronomical imaging with optical long-baseline interferometers in the mid-infrared (MIR) domain aims to reach to very high angular resolutions in the range of 10 mas (Monnier et al. 2014; Matter et al. 2016). Observations in the *L*, *M* and *N* astronomical bands ranging from 2.5 µm to 13 µm would allow us to study challenging science cases such as protoplanetary disks or Active Galactic Nuclei. Unfortunately, the observations in these spectral bands raise many technological difficulties in terms of beam transport, spatial filtering and above all low flux detection. With a classical interferometric instrument, the thermal background radiated by the whole transmission chain makes it difficult to extract the astronomical signal (Perrin et al. 2003).

To overcome this experimental drawback, we have been developing for ten years a new instrumental concept called Astronomical Light Optical Hybrid Analysis (ALOHA) (Brustlein et al. 2008). In this approach, the MIR astronomical signal collected by each telescope is frequency shifted to the visible or near infrared domain before coherent transport and interferometric combination in order to carry out the spatial coherence analysis. In each arm of the interferometer, this frequency shift is obtained by a sum frequency generation (SFG) process (Boyd 2008), where the MIR astronomical signal at the wavelength λ_s is coupled into a non-linear crystal together with a strong pump wave at λ_p. The non-linear interaction leads to the generation of a converted signal with a shorter wavelength λ_c, while preserving the coherence properties of the MIR radiation. The use of optical waveguides over the SFG in the non-linear crystals and coherent transport and combination of the radiations in single-mode guided components ensures a very good spatial filtering mandatory for fringe contrast calibration (Coudé du Foresto et al. 1997).

In a recent proof of principle experiment with an astronomical signal centred around 1.55 µm, we obtained first fringes on the sky with the Center for High Angular Resolution Astronomy (CHARA) Array (Darré et al. 2016). In the meantime, we developed in laboratory a version of ALOHA working in the *L* band at 3.39 µm. In a preliminary laboratory experiment, we obtained the first fringes with a bright quasi monochromatic source (He–Ne laser) with a high fringe contrast (Szemendera et al. 2016).

In this paper, we experimentally study the limiting sensitivity of ALOHA@3.39 µm with a quasi-monochromatic source. We evaluate the contrasts of the recorded fringe patterns in the photon counting regime for always fainter MIR input powers. The reliability of the contrasts is assessed by measuring the signal-to-noise ratio (SNR).

★ E-mail: francois.reynaud@unilim.fr

2 GENERAL DESCRIPTION OF THE ALOHA@3.39 µm INTERFEROMETER

The general sketch of our in-lab experimental set-up is shown in Fig. 1. It is divided in three main subsystems. The 3.39 µm stage acts as the two collecting telescopes of a real array, and provides a spatially coherent and collimated beam to each arm of the interferometer. The MIR signal is produced by a Continuous Wave He–Ne laser emitting a quasi-monochromatic radiation around λ_s = 3.39 µm. It can be attenuated by optical densities to set a signal power between 3 pW and 100 fW at the input of each interferometric arm. The MIR signal is then sent to the non-linear stage thanks to mirrors.

In the SFG stage, the incoming MIR light is frequency converted thanks to 90 mm-long Periodically Poled Lithium Niobate (PPLN) crystals. The MIR signal propagates in low-loss, single-mode Ti-indiffused waveguides. The non-linear process is powered by a monochromatic laser at λ_p = 1064 nm emitted by a distributed feedback laser (DFB) and shared between the two interferometric arms. The converted wave is generated at λ_c = 810 nm through the SFG process. To achieve repeatable characteristics of conversion efficiency, the PPLN waveguide samples were operated at temperatures above 130 °C to prevent any photorefractive effect. The poling period of the PPLN waveguides is equal to 21.8 µm and allows the quasi-phase-matching of the SFG process at the operating temperature. Due to the weak guidance conditions, it is necessary to adapt the pump beam geometry for an optimal spatial overlapping with the spatial mode of the MIR signal. The pump wave is then back injected at the output face of the PPLNs thanks to a waveguide taper. After propagating in the reverse direction, the pump wave is reflected by a dichroic coating on the input face of the crystals (Anti-Reflection at 3.39 µm and High-Reflection at 1064 nm). Then it copropagates with the MIR signal leading to the generation of a converted wave at 810 nm by SFG.

At the output of each PPLN crystal the beams reach the 810 nm stage. These converted beams are injected into two 4 m long silica optical fibre at 810 nm acting as spatial filters. All the guided components of the 810 nm stage are single-mode and polarization maintaining at the converted wavelength. This ensures a stable and well calibrated interferometric signal.

Fibre delay lines allow us to operate around the zero optical path difference to optimize the fringe contrast. Notice that in our particular experimental configuration, their adjustment is not critical since the converted fields are quasi-monochromatic. However, for a broad-band input signal around 3.39 µm, the coherence length of the converted beam would be equal to 3.8 mm (this value directly depends on the spectral acceptance $\delta\lambda$ = 3 nm of the non-linear crystals). In that case, a fine tuning of the delay lines with a 0.1 mm accuracy would be mandatory.

On one arm of the interferometer, a piezoelectric fibre optical path modulator is driven by a triangular voltage function (±150 V span) to temporally display the fringe pattern. The stroke of this fibre stretching is in the range of 20 µm, much less than the coherence length of the converted fields. This optical path variation allows us to record 25 fringes over the acquisition time of each frame.

The coherent combination of the two converted fields is performed thanks to a single-mode and polarization maintaining coupler at 810 nm. At the output of this fibre coupler, the converted interferometric signal is spectrally cleaned up through three notch filters centred at 810 nm, in order to reject parasitic signals such as frequency doubling of the pump at 532 nm and the residual signal of pump.

For a 100 mW pump power, the power conversion efficiency of each non-linear crystal is in the range of $1.5 \cdot 10^{-5}$ at maximum. Although the conversion efficiency is directly proportional to the pump power, its value has been limited to 100 mW to avoid damaging the input face of the non-linear waveguides. Note that this overall throughput takes into account the non-linear conversion efficiency, but also the stringent spatial and spectral filtering and the whole losses resulting from the injection and collimating stages.

The interferometric signal is then detected by an Si-APD photon counter. The frame duration of the acquired signal is set to τ = 400 ms. The electrical output signal is temporally sampled at 200 kHz by a National Instruments acquisition system controlled by a LabVIEW VI.

3 DATA PROCESSING

In the photon counting regime, each frame consists of a set of electrical pulses related to the photon probability distribution, i.e. the intensity of the fringe pattern. Thus, the raw data consists of a set of frames of binary functions $X_i(t)$ each recorded over the constant acquisition time τ.

Each frame is individually processed by a Fast Fourier Transform (FFT) to get

$$\widetilde{X}_i(f) = \mathrm{FFT}[X_i(t)]. \quad (1)$$

In our experimental framework, a random fluctuation of the fringe pattern position between frames is due to the uncontrolled experimental environment. To overcome this piston error, we perform an incoherent integration by stacking the Power Spectral Density (PSD) squared modulus of each frame.

$$\langle \mid \widetilde{X}(f) \mid^2 \rangle \quad = \quad \frac{1}{N} \sum_{1}^{N} \mid \widetilde{X}_i(f) \mid^2, \quad (2)$$

where N is the number of frames over which the integration is achieved. Nevertheless, in the photon counting regime, the converted signal measurement is perturbed by a global quantum noise arising from mainly two sources. The first one is related to the photons coming from the observed source and up-converted through the non-linear stage. The second noise contribution is related to the dark count, including:

- the intrinsic Avalanche photodiode (APD) silicon detector dark count in the range of 20 counts/s,
- the bias counts optically generated by a cascade of spontaneous parametric down-conversion of the pump (Pelc et al. 2011),
- the photon-events produced by conversion of the thermal radiation emitted by the optical components upstream of the PPLN crystals.

In our experiment, the mean number of global dark counts is in the range of $\langle DC \rangle$ = 90 counts/s for a pump

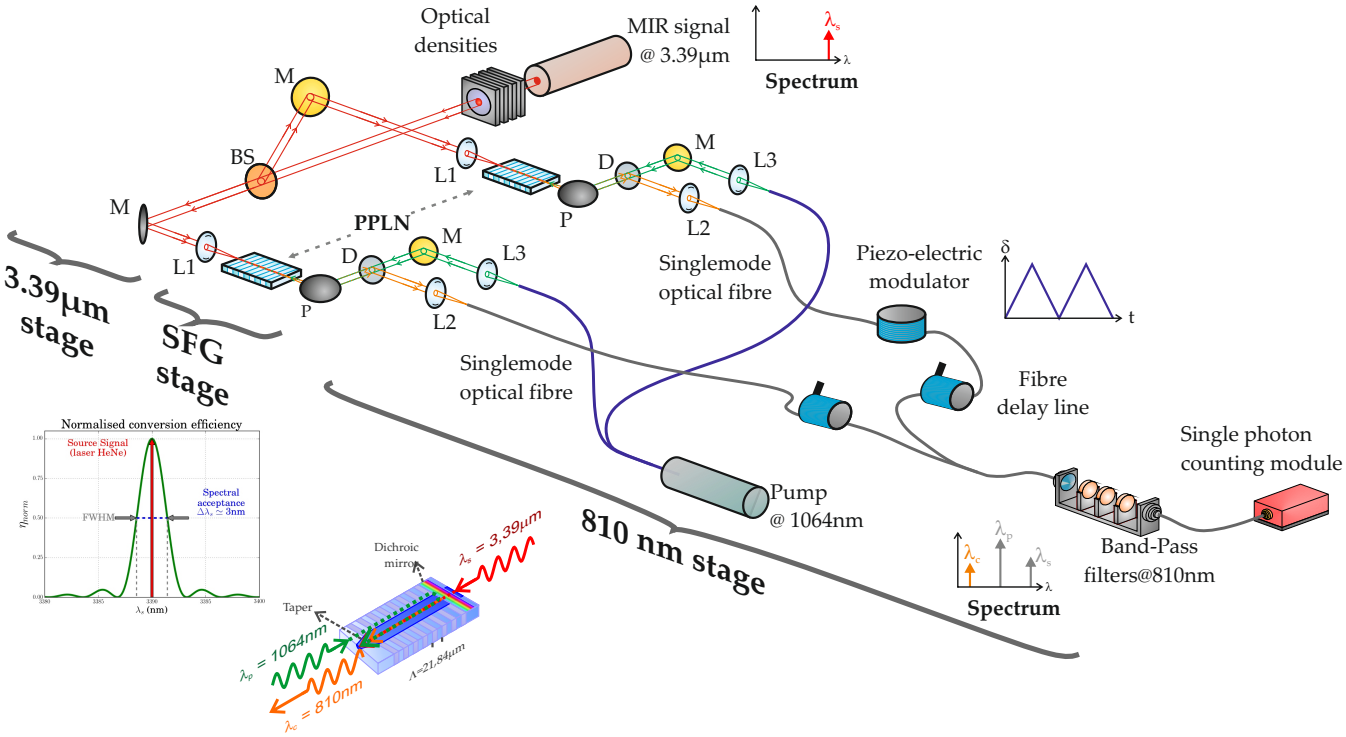

Figure 1. Description of the experimental setup. M: injection mirrors for the infrared signal at 3.39µm ; BS: beam splitter used to separate the MIR signal in two separated ways ; L1: focusing lens for the MIR injection into the PPLN waveguide; L2: focusing lens for the converted signal into a fibre single mode at 810 nm; L3: collimating lens for the pump signal; P: off-axis parabola ; D: dichroic mirror used to separate converted signal from pump signal. Left-most inset: theoretical normalized conversion efficiency curve. Left inset: PPLN injection scheme

power close to 100 mW per PPLN. For a source flux close to 1 pW, the mean number of detected photons after frequency conversion and coherent propagation in the interferometric arms is approximately $\langle N_{h\nu}\rangle = 120$ photons/s. These independent noise contributions lead to the generation of a white noise background in the PSD over the integration process as shown in Fig. 2. This background is equal to the mean value of the number N_c of counts per frame:

$$\langle N_c\rangle = \langle N_{h\nu}\rangle + \langle DC\rangle. \quad (3)$$

Finally, the PSD values at the zero frequency and at the modulation frequency of the fringes f_0 are written:

$$\begin{aligned} \langle |\widetilde{X}(0)|^2\rangle &= (\langle N_{h\nu}\rangle + \langle DC\rangle)^2 + \langle N_c\rangle \\ \langle |\widetilde{X}(f_0)|^2\rangle &= C^2.\langle N_{h\nu}\rangle^2 + \langle N_c\rangle, \end{aligned} \quad (4)$$

where C is the fringe contrast to measure.

To monitor the fringe detection over the PSD integration process, we compute the SNR defined as:

$$\mathrm{SNR} = \frac{\langle |\widetilde{X}(f_0)|^2\rangle - \langle N_c\rangle}{\mathrm{RMS}\left(\langle |\widetilde{X}(f)|^2\rangle\right)} \quad \text{where } f \neq (0, f_0). \quad (5)$$

$\mathrm{RMS}\left(\langle |\widetilde{X}(f)|^2\rangle\right)$ is the noise estimated as the fluctuation of the PSD continuous background at the frequencies different from 0 and f_0. This figure of merit corresponds to the SNR of the fringe peak amplitude, and evolves as a function of the square root of the number of frames.

Finally, the experimental fringe contrast C can be computed by using the following expression:

$$C = \frac{\sqrt{\langle |\widetilde{X}(f_0)|^2\rangle - \langle N_c\rangle}}{\sqrt{\langle |\widetilde{X}(0)|^2\rangle - \langle N_c\rangle - \langle DC\rangle}}. \quad (6)$$

4 EXPERIMENTAL RESULTS

We have recorded time interferograms at the output of the interferometer for different MIR input powers. For each flux level of the MIR source, several steps are necessary to measure the fringe contrast:

- First, without any MIR signal source and only the pump source propagating in the PPLN waveguides, we acquire 600 frames in order to estimate the mean number of dark counts $\langle DC\rangle$;
- Second, we determine the mean number of up-converted photons detected at the interferometer output of each arm. This allows us to determine the correction factor of the contrast due to the photometric imbalance;
- Finally, we acquire the interferometric frames with an integration time ranging from 4 to 16 minutes depending on the MIR flux level.

The experimental results are reported in Table 1. The contrasts are unbiased from the effects of the photometric imbalance.

Fig. 3 (left) presents the normalized experimental PSD

P_S (pW)	$\langle DC \rangle$ (counts/sec)	$\langle N_{h\nu} \rangle_1$ (ph/sec)	$\langle N_{h\nu} \rangle_2$ (ph/sec)	Number of frames	Integration time (min.)	Contrast %	SNR
2.6	91.0	131	182	600	4.0	96.8	507
1.2	91.0	63	87	600	4.0	95.5	186
0.6	92.0	32	45	600	4.0	98.5	75
0.15	92.5	7.0	9.8	1700	11.3	94.5	7.4
0.1	94.0	5.5	7.8	2400	16.0	94.9	6.8

Table 1. Summary of the experimental results achieved, with P_S the MIR flux level at each input of the interferometric arms, $\langle DC \rangle$ the mean number of dark counts and $\langle N_{h\nu} \rangle_i$ the mean number of the photons detected at the interferometer output #i. The values of the contrasts and the SNR are obtained after integration of the power spectral density of the frames. The frame duration is equal to 400 ms.

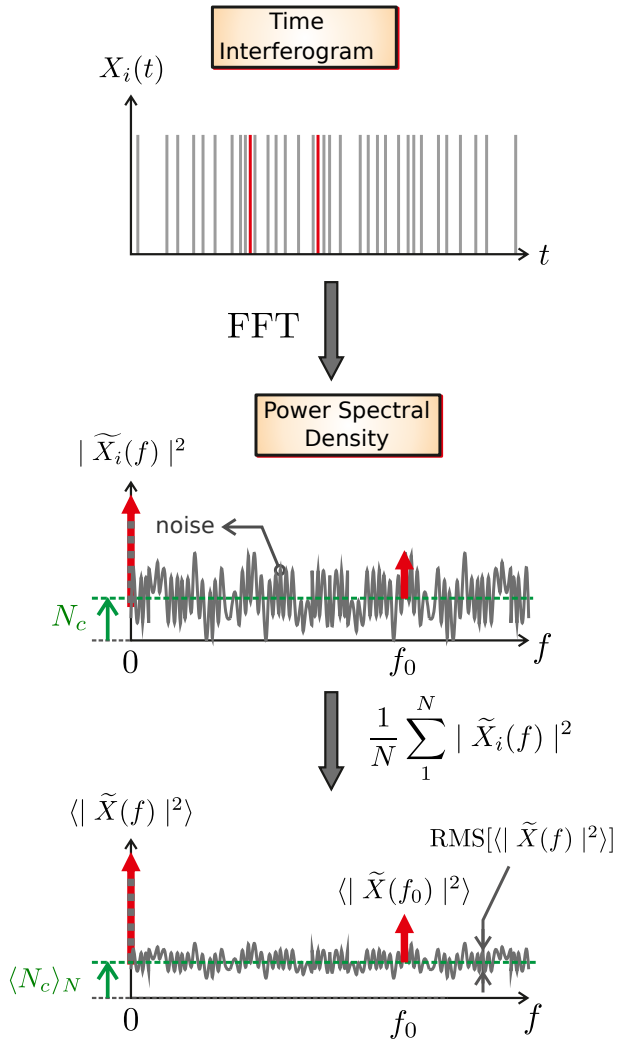

Figure 2. Data reduction process. A set of Power Spectral Densities is obtained from the Fast Fourier Transform of each frame (time interferogram), and then is integrated to enhance the SNR.

obtained after integration for different MIR flux levels. In each case, the fringe peak is clearly visible in spite of the fluctuations of the background due to the quantum noise. From these curves and equations (4), we plot the C^2 estimator as a function of the spectral channel (Fig. 3, right).

Fig. 4 shows the evolution of the SNR and the contrasts over the PSD integration. We experimentally verify that the SNR has a square root evolution as a function of the number of frames. When the number of photons is close to, or greater than the number of dark counts, the fringe peak is easily observable from the very first recorded frame. For any flux level, the fringe contrast measured gradually tends to be close to 97%, but the integration time required is all the more important as the number of photons is low.

In addition, we are able to measure a fringe peak with less than 100 fW MIR input power. In this case, we obtain an SNR of 7 after an integration time of 16 min (2400 frames). This result shows the potential to get high contrasted fringes with very low MIR input flux.

5 CONCLUSION

To address the MIR domain in the framework of the ALOHA project, we are developing a laboratory up-conversion interferometer operating at 3.39 µm, where an SFG process is implemented in each arm of this instrument. We observed fringes and estimated the related contrasts in the *L* band with MIR flux levels at the input of each interferometric arm down to 100 fW. In this latter case, the SNR was almost equal to 7.

In its current state, even with the limited performances of the SFG stages, the ALOHA@3.39 µm prototype should be able to get fringes and to measure contrasts on a star of magnitude equal to 0 in the *L* Band with a 1 m^2 telescope surface and a converted spectral bandwidth close to 3 nm centred around 3.39 µm (corresponding to a spectral resolution equal to 1100). These promising experimental results prove that the ALOHA concept is fully relevant for future astrophysical applications in the MIR spectral domain.

The main potential improvement would be increasing the conversion efficiency. The Ti-indiffused PPLN waveguide samples used in our experiment exhibit a low conversion efficiency due to the poor spatial modes overlapping between the fields at very different wavelengths (Kurimura et al. 2006). Moreover, they require high operating temperature necessary to strongly mitigate the photorefractive perturbations. In recent years, a new technology so-called ridge PPLN has been developed to overcome these limitations (Umeki et al. 2010; Chauvet et al. 2016). Using this waveguide technology, we expect an enhancement of the conversion efficient by several orders of magnitude. In order to mimic the real astronomical conditions we plan to replace the He–Ne laser by a blackbody to perform fringe contrast measurements with a faint source emitting a broad-band spectrum around 3.39 µm.

In a more general outlook, the ALOHA concept addresses the issue of thermal noise in a MIR interferometer. By performing SFG as close as possible to the telescope

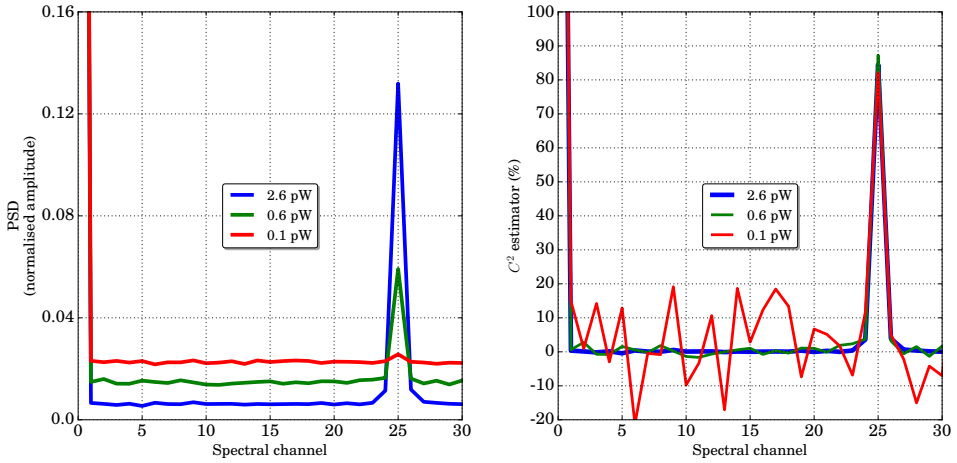

Figure 3. Left: normalized PSD obtained after integration over time for 3 different MIR input powers. Right: C^2 estimator as a function of the spectral channel derived from the normalized PSD and equations (4). Integration time for each MIR input power is given in Table 1.

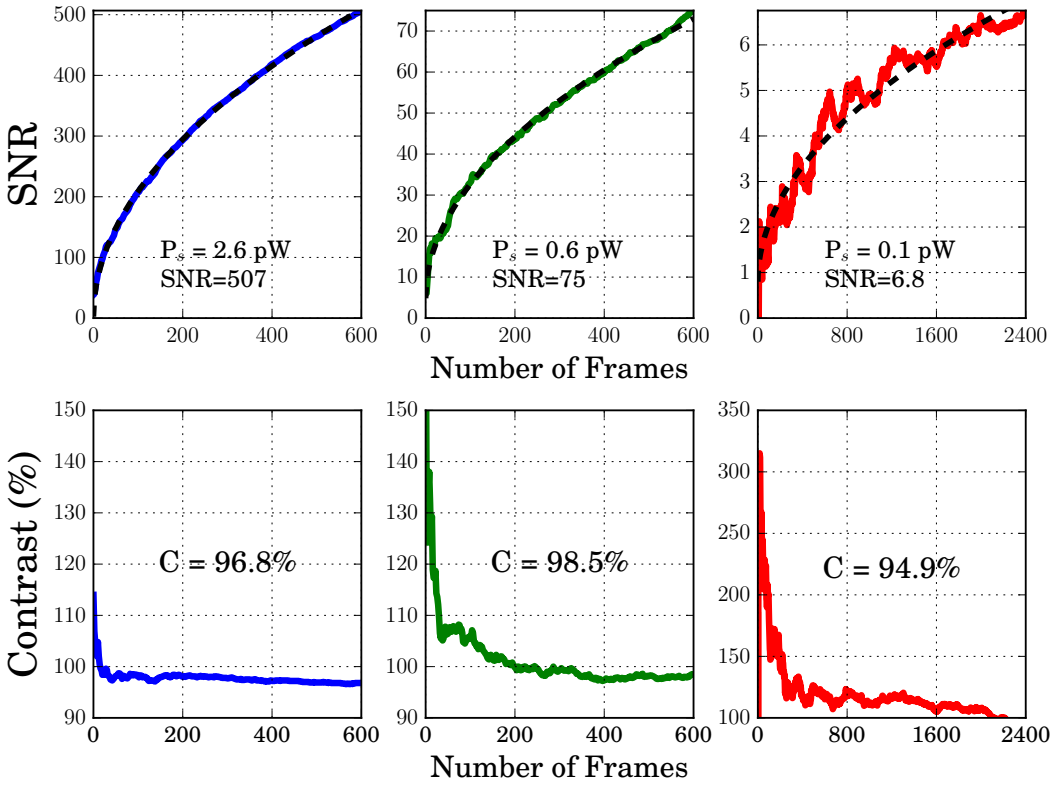

Figure 4. Top: square root SNR evolution as a function of the frame number for different MIR input flux. Bottom: Plot of the corresponding estimated contrasts.

focus, the converted beam would not undergo any further thermal background generated by the whole optical chain present in a classical scheme. In this way, we could extend the number of interferometric arms without any tremendous increase of the thermal noise background. Finally, the use of silica single mode fibre to carry out the beam coherent transport allows us to envision kilometric interferometer, giving access to unprecedented high angular resolution astronomical imaging in the MIR domain.

ACKNOWLEDGEMENTS

This work has been financially supported by the Centre National d'Études Spatiales (CNES), the Institut National des

Sciences de l'Univers (INSU), Airbus Group and the Région Limousin. We gratefully acknowledge Wolfgang Sohler and Harald Herrmann (Universität Paderborn) for the supply of the non-linear crystals and many helpful and stimulating discussions. Our thanks go also to Alain Dexet for the development and his advices for all the specific mechanical components.

References

Boyd R. W., 2008, Nonlinear Optics, 3 edn. Academic Press, Amsterdam ; Boston

Brustlein S., Del Rio L., Tonello A., Delage L., Reynaud F., Herrmann H., Sohler W., 2008, Phys. Rev. Lett., 100, 153903

Chauvet M., Henrot F., Bassignot F., Devaux F., Gauthier-Manuel L., Pêcheur V., Maillotte H., Dahmani B., 2016, Journal of Optics, 18, 085503

Coudé du Foresto V., Ridgway S., Mariotti J.-M., 1997, A&AS, 121

Darré P., et al., 2016, Phys. Rev. Lett., 117, 233902

Kurimura S., Kato Y., Maruyama M., Usui Y., Nakajima H., 2006, Applied Physics Letters, 89

Matter A., et al., 2016, in Society of Photo-Optical Instrumentation Engineers (SPIE) Conference Series. p. 99070A (arXiv:1608.02350), doi:10.1117/12.2233052

Monnier J. D., et al., 2014, in Optical and Infrared Interferometry IV. p. 914610 (arXiv:1407.7032), doi:10.1117/12.2057262

National Instruments 2015, Test, Measurement, and Embedded Systems, http://www.ni.com/

Pelc J. S., Ma L., Phillips C. R., Zhang Q., Langrock C., Slattery O., Tang X., Fejer M. M., 2011, Opt. Express, 19, 21445

Perrin G., Leinert C., Graser U., Waters L. B. F. M., Lopez B., 2003, in Perrin G., Malbet F., eds, EAS Publications Series Vol. 6, EAS Publications Series. p. 127, doi:10.1051/eas:2003010

Szemendera L., Darré P., Baudoin R., Grossard L., Delage L., Herrmann H., Silberhorn C., Reynaud F., 2016, MNRAS, 457, 3115

Umeki T., Tadanaga O., Asobe M., 2010, IEEE Journal of Quantum Electronics, 46, 1206

This paper has been typeset from a TEX/LATEX file prepared by the author.